Article:
Rabizadeh, T, Peacock, CL orcid.org/0000-0003-3754-9294 and Benning, LG orcid.org/0000-0001-9972-5578 (2020) Investigating the Effectiveness of Phosphonate Additives in Hindering the Calcium Sulfate Dihydrate Scale Formation. Industrial & Engineering Chemistry Research, 59 (33). pp. 14970-14980. ISSN 0888-5885

https://doi.org/10.1021/acs.iecr.0c03600

Investigating the effectiveness of phosphonate additives in hindering the calcium sulfate dihydrate scale formation

Taher Rabizadeh[1,2*], Caroline L. Peacock[2], Liane G. Benning[2,3,4]

1- Department of Materials Engineering, Faculty of Mechanical Engineering, University of Tabriz, 51666-16471, Tabriz, Iran

2- School of Earth and Environment, University of Leeds, Leeds, LS2 9JT, United Kingdom

3- GFZ, German Research Centre for Geosciences, Telegrafenberg, 14473 Potsdam, Germany

4- Department of Earth Sciences, Free University of Berlin, 12249 Berlin, Germany

* Correspondence to: Taher Rabizadeh (t.rabizadeh@tabrizu.ac.ir)

Abstract

The effects of 20 ppm 1-Hydroxy Ethylidene-1,1-Diphosphonic Acid (HEDP), Amino Trimethylene Phosphonic Acid (ATMP), Polyamino Polyether Methylene Phosphonic Acid (PAPEMP), Diethylene Triamine Penta (Methylene Phosphonic Acid) (DTPMPA) and Bis(HexaMethylene Triamine Penta (Methylene Phosphonic Acid)) (BHMTPMPA) on the room temperature crystallization of calcium sulfate dihydrate (gypsum) were investigated by by *in situ* UV-Vis, XRD, XPS, ICP-OES, and SEM. Comparison between the additive-containing and additive-free experiments showed that BHMTPMPA was the most efficient antiscalant by completely inhibiting crystallization. Due to the chain length of the BHMTPMPA molecule, the crystallization kinetics decreased to a larger extent than

DTPMPA. The increase in pH of the solution from ~ 4 to ~ 7, positively enhanced the efficiency of the phosphonates in inhibiting crystallization. Our results revealed that partially deprotonated phosphonate additives were strongly associated with gypsum crystals and / or potentially taken up into the crystal matrix resulted in a sudden and sharp increase in turbidity plots. Furthermore, phosphonate additives altered the thin, twinned gypsum crystals into thick needles.

Keywords: crystallization; calcium sulfate dihydrate; antiscalants; phosphonates; adsorption; X-ray Photoelectron Spectroscopy.

1. Introduction

Mineral scale formation is a major problem in many industrial processes such as crude oil production, reverse osmosis desalination, cooling systems, papermaking, etc.[1-4] These unfavourable minerals that usually deposit in pipes, membranes, heat exchangers, and mixing tanks cause a considerable reduction in fluid flow and blockage of the pipelines, and other equipment, together with other consequences like corrosion.[5-8]

There are various types of minerals that form scales. Among these, calcium carbonate[9,10], barium sulfate[11], magnesium hydroxide[12], silica[13,14], and calcium sulfate[15,16] are frequent. In the calcium sulfate system, calcium sulfate dihydrate (gypsum, $CaSO_4 \cdot 2H_2O$) commonly precipitates in industrial systems[17], and its formation and solubility are controlled by different parameters such as temperature, supersaturation, and impurities.[1] Most importantly, gypsum as a mineral scale is highly stable and its formation is pH-independent.[18] Therefore, it is hard to remove by industrial scale removal techniques such as acid washing or mechanical cleaning.[19] Furthermore, cleaning and / or mechanical removal of mineral scales is undesirable, as it is costly and affects the performance and efficiency of industrial units. [20,21]

It is, therefore, desirable to mitigate or reduce mineral scaling rather than remove the calcium sulfate scale mineral.

In this regard, addition of chemicals such as phosphonates, carboxylates and sulfonates, known as inhibitors (or antiscalants), is more economical and effective than, for example, acid cleaning or mechanical methods.[22,23] Commonly used industrial inhibitors are basically divided into nonpolymeric[24,25] and polymeric [26,27] ones, and their role in tackling mineral scaling is still under debate.[1] A fundamental understanding of how industrial antiscalants operate is slowly emerging, yet the operation and efficiency of phosphonate antiscalants, in particular, is still not well-understood. With respect to the calcium sulfate scale system, studies that evaluated the effects of phosphonate additives on calcium sulfate formation have so far focused on effect these antiscalants have on changing the precipitation onset.[28] In other scale systems, studies attempted to derive a more mechanistic understanding of the role of phosphonate antiscalants, yet many unanswered questions still remain. For example, in the calcium carbonate (calcite) scale system, molecular modelling has shown that among phosphonate additives with different molecular structure, just monophosphonates incorporates into the calcite structure[29], while HEDP only interacted with the calcite surface at step sites.[30] Furthermore, in the barium sulfate and calcium carbonate systems, the inhibitory efficiency of Diethylene Triamine Penta (Methylene Phosphonic Acid) (DTPMPA) on barite[31] and calcite[32] scale formation are in both cases lower than that of the poly-phosphino carboxylic acid, yet what the driving mechanism is still unclear. This applies also to the calcium sulfate system, where a fundamental mechanistic understanding of the effects of different phosphonates on calcium sulfate scale formation is totally lacking. The questions of how these inhibitors operate, interact or change the way calcium sulfate crystals form and how they can be further optimised to reduce or mitigate mineral scaling, are still open.

In this research, we assessed the effects of five industrial phosphonate antiscalants on the nucleation and growth kinetics of calcium sulfate dihydrate, gypsum, and evaluated if and how these antiscalants may change the morphology of the forming gypsum crystals. We followed the processes through analyses of changes in both, the reacting solution and the forming solids simultaneously. For the first time, we quantify the different trends in the kinetics of gypsum crystallization and demonstrate the surface adsorption and / or structural incorporation of the antiscalants using a combination of X-ray photoelectron spectroscopy (XPS), and inductively coupled plasma optical emission spectrometry (ICP-OES) analyses. Our results show the significant impact of antiscalant functional group characteristics on the efficiency of the inhibitor in delaying gypsum nucleation and growth. Furthermore, we document how this interaction also caused changes in the resulting gypsum crystal morphologies.

2. Experimental methods

To produce calcium sulfate dihydrate crystals, 500 mL of a 200 mM $CaCl_2 \cdot 2H_2O$ solution (100 % AnalaR Normapour VWR) and a 200 mM Na_2SO_4 solution (100 % AnalaR Normapour; VWR) were mixed in a 1000 mL reactor (yielded a solution with a supersation of 0.84 calculated with the geochemical computer code PhreeqC 3.3.3was obtained[33]) at 21 ˚C and under constant stirring condition.

1-Hydroxy Ethylidene-1,1-Diphosphonic Acid (HEDP), Amino Trimethylene Phosphonic Acid (ATMP), Polyamino Polyether Methylene Phosphonic Acid (PAPEMP), Diethylene Triamine Penta (Methylene Phosphonic Acid) (DTPMPA) and Bis(HexaMethylene Triamine Penta (Methylene Phosphonic Acid)) (BHMTPMPA) with the molecular structure depicted in Figure 1 were provided by Shandong Taihe Water Treatment Technologies Company. 40 ppm of the phosphonate additives were added to the Na_2SO_4

99 solution prior to the addition of the $CaCl_2 \cdot 2H_2O$ solution. Therefore, there were 100 mM
100 calcium, 100 mM sulfate and 20 ppm phosphonates initially after mixing solutions. The pH
101 of the calcium sulfate dihydrate crystallization solution was adjusted to pH to ~ 4 or ~ 7, with
102 NaOH and / or HCl.[34]
103

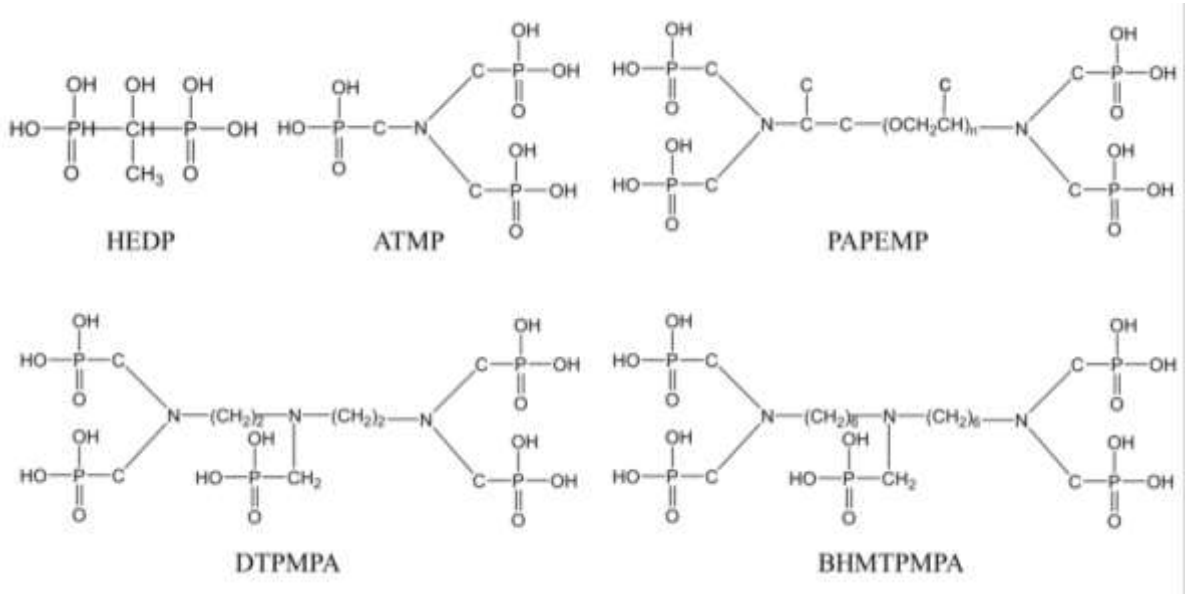

104

105 Figure 1.Molecular structure of the tested phosphonate additives.
106

107 Changes in the calcium sulfate dihydrate crystallization solutions were tracked by
108 monitoring the increase in absorbance using a UV-vis spectrophotometer (Uvikon XL) at λ =
109 520 nm with the angle between the incident beam and detector of 180˚. The crystallization
110 reactions were followed at 21 ˚C for up to 240 minutes by recording the changes in the
111 absorbance of 2.5 mL aliquots taken from the gypsum precipitation solutions. These
112 procedures were repeated in triplicate and the acquired absorbance data were plotted as the
113 normalized changes in solution turbidity over 240 minutes. It is noteworthy that when a UV-
114 vis spectrophotometer is used to measure the turbidity variation as a proxy to the
115 crystallisation kinetics, a few points have to be considered. For example, the Beer-Lambert
116 law is applied to dilute solutions and at concentrated solutions the absorbance plot deviates

from linear behaviour [35]; any chemical changes during the crystallisation (e.g., dissociation-association) affects the absorbance[36]; reflection and scattering the light by the surface of the growing crystals may affect the measured absorbance[37], etc.[34]

The crystals precipitated in the absence or presence of phosphonate additives were always calcium sulfate dihydrate as confirmed by powder X-ray diffraction (XRD; Bruker D8 diffractometer; CuKα1). The morphology of the precipitated crystals was studied using a field emission gun scanning electron microscope (FEG-SEM, FEI Quanta 650, 5 kV).

To quantify the association between the phosphonate molecules and the precipitated crystals, a few milligram of the formed end-products were dissolved in 2% nitric acid (69% AnalaR Normapour analytical reagent) and the resulting solutions together with aliquots taken from the crystallization solution after 10 seconds (initial concentration) and 240 minutes (end concentration) were analyzed for their Ca and P contents by inductively coupled plasma optical emission spectrometry (ICP-OES; Thermo Scientific iCAP 7400; with a limit of detection and uncertainties of 0.004 and 2%, respectively for Ca^{2+} and 0.007 ppm and 3.78%, respectively for P).[34] To determine whether the phosphonate additive were surface adsorbed and / or structurally incorporated into gypsum crystals, 1.5 grams of the end-products were suspended in a 200 ml saturated gypsum solution for 2 hours under continuous stirring to desorb any potentially surface adsorbed phosphonate additives. The saturated gypsum solution was prepared by equilibrating gypsum (puriss, 99.0-101.0%, Sigma-Aldrich) in Milli-Q water at pH ~ 9 and filtering through 0.2 µm syringe filters prior to desorption. After this step the remaining crystals were dissolved in 2% nitric acid and the solutions were analyzed for P concentration as described above. The amount of the inhibitors associated with the formed crystals (association amount; $C_{A,inhibitor}$) before and after desorption were determined from the concentration of inhibitor (ppm) (calculated based on the phosphorous

element concentration measured in the full digestion solutions) divided by the total amount of crystals dissolved in the solution (ppm).[34]

Finally, the surface interactions between the inhibitors and the formed end-products, were determined by X-ray photoelectron spectroscopy (XPS; Kratos Axis Ultra-DLD spectrometer; detection limit of 0.1 at. %). Each XPS spectrum was recorded from the top layers (8-10 nm) of the gypsum crystals. A monochromatic aluminium K_α X-ray source (144 W) and pass energies of 40 eV (high resolution scans) was utilized. The base pressure during analysis was ca. 6×10^{-7} Pa. All spectra were referenced to the C (1s) signal at 284.8 eV. CasaXPS^{TM} (Version 2.3.15) was employed to quantify all data as atomic percentage and considering the elemental sensitivity factors provided by the manufacturer.

3. Results

In the additive-free experiments, at either pH ~ 4 or ~ 7, the turbidity of the solution changed after ~ 30 seconds (called hereafter the induction time; the point where the baseline deviated from the zero value[38]) and within ~ 30 minutes it reached turbidity of 100% (Figure 2). However, in each of the phosphonate-containing experiments and at pH ~ 4, the induction times increased and it took longer to reach a maximum turbidity plateau. At a constant concentration (20 ppm) of antiscalants and pH ~ 4, the induction time increased 4 fold (to ~ 2 minutes), 36 fold (to ~ 18 minutes), 60 fold (to ~ 30 minutes), and 140 fold (to ~ 70 minutes) in the presence of HEDP, ATMP, PAPEMP and DTPMPA, respectively. The slope of the turbidity curves decreased and the crystallization end-plateaus were reached only in the presence of HEDP (after ~ 65 minutes) and ATMP (after ~ 100 minutes). The most remarkable effect was recorded in the presence of BHMTPMPA, where no turbidity change was observed even after long time periods.[34]

At a higher pH (~ 7), the effects of 20 ppm additive were strikingly different. No change in turbidity was recorded for any of the additives, except for HEDP (Figure 3). In the presence of HEDP the elapsed time before the onset of turbidity was ~ 30 minutes (15 times longer than in the pH ~ 4 experiments at equivalent concentration). Noticeable also is the fact that the turbidity developed with a different trend than in the phosphonate-free system, in that up to ~ 75 minutes the turbidity increased with a constant slope until it reached ~ 3 %, after which, the turbidity sharply increased with the curve having a slope similar to the additive-free system and reaching a plateau within the next ~ 50 minutes (~ 130 minutes from beginning).[34]

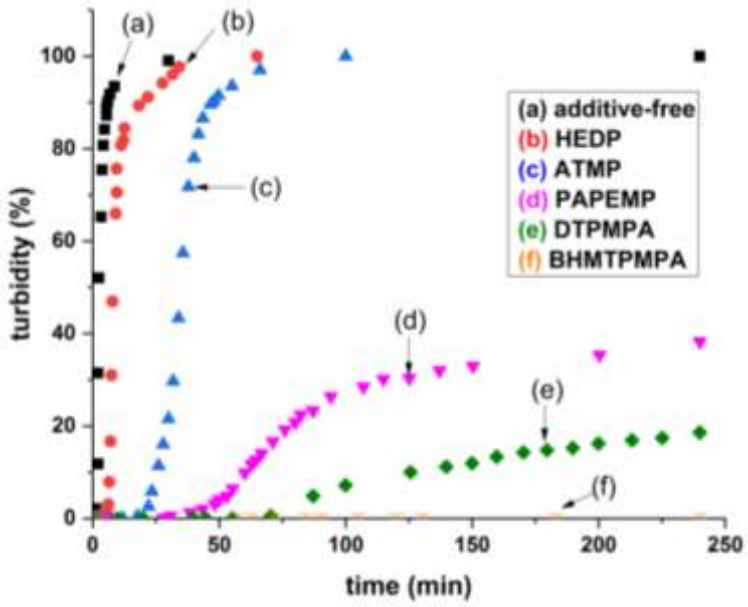

Figure 2. Turbidity curves plotted as a function of time in the absence and presence of 20 ppm HEDP, ATMP, PAPEMP, DTPMPA and BHMTPMP at pH ~ 4.[34]

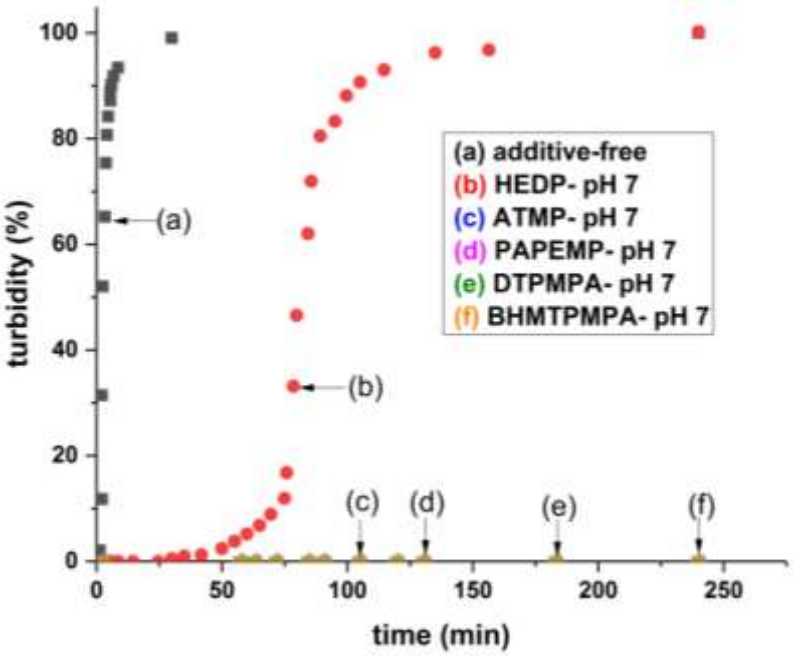

Figure 3. Turbidity curves plotted as a function of time in the absence and presence of 20 ppm HEDP, ATMP, PAPEMP, DTPMPA, BHMTPMPA at pH ~ 7.[34]

Changes in concentration of the antiscalants during gypsum crystallization were analyzed by measuring their initial (after ~ 10 seconds; ~ 20 ppm inhibitor) and end concentrations (after 240 minutes) of reaction (Figure 4). At pH ~ 4, no decrease in the HEDP and BHMTPMP concentrations were measured, but the concentrations of ATMP, PAPEMP and DTPMPA decreased by 18 ± 1 ppm, 10 ± 1.2 ppm and 7 ± 1 ppm. At pH ~ 7, no decrease in the inhibitors' concentrations was observed even after 240 minutes, except for HEDP which was fully removed. This decrease in HEDP inhibitor concentration was mirrored by a reverse trend in the turbidity profile (Figure 5).[34]

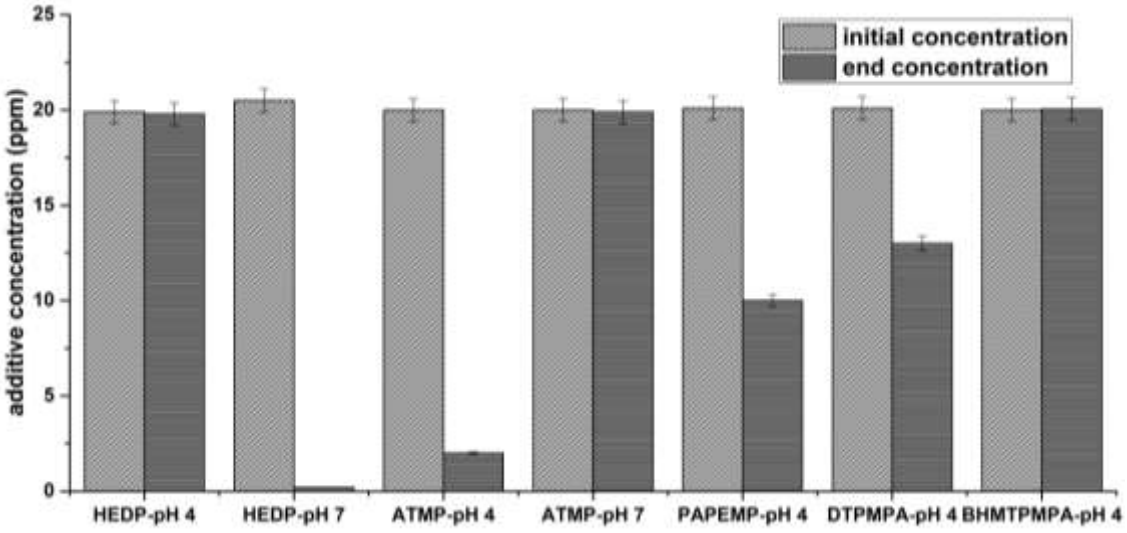

Figure 4. Initial and end concentrations of HEDP, ATMP, PAPEMP, DTPMPA and BHMTPMP in the experimental solutions at pH ~ 4 and ~ 7.[34]

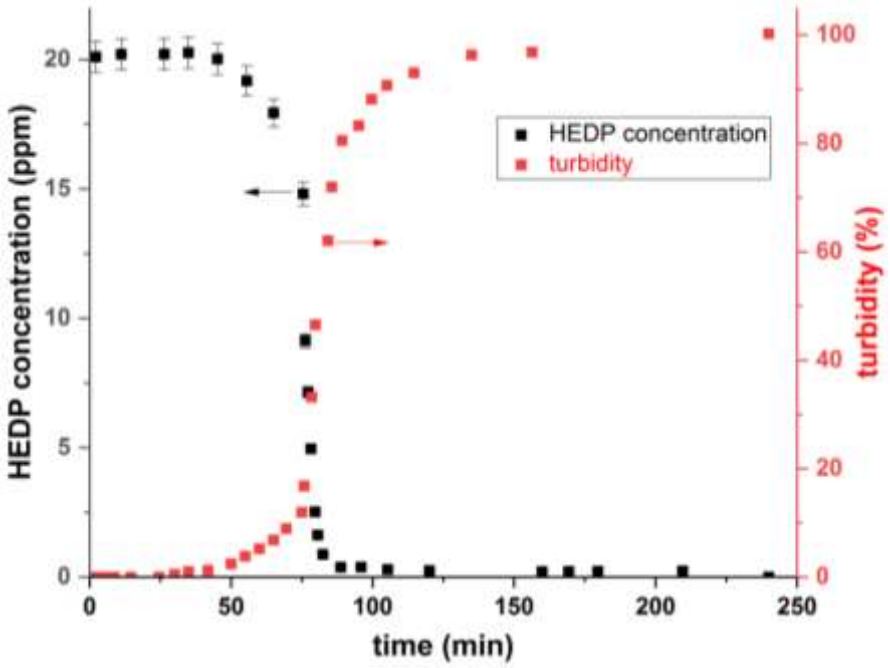

Figure 5. Changes in turbidity and HEDP concentration in the gypsum crystallization solution carried out in the presence of 20 ppm HEDP over 240 minutes at pH ~ 7.[34]

The concentration of Ca^{2+} in the crystallization solution after ~ 10 seconds (starting concentration) and 240 minutes (end concentration) was also measured. As can be seen from Table 1 in the additive-free system from the initial 100 mM Ca^{2+}, ~ 72 ± 1.4 mM of Ca^{2+} were consumed at the end of the reaction. However, in the presence of 20 ppm of the most

effective inhibitor (BHMTPMPA) at pH ~ 4, ATMP, PAPEMP, and DTPMPA at pH ~ 7, Ca^{2+} was not depleted in the crystallization solution, while in the presence of HEDP at pH ~ 7, ~ 59 ± 1.2 mM of Ca^{2+} was consumed to produce gypsum crystals. These results cross correlate with our turbidity measurements where no gypsum was observed in the presence of BHMTPMPA at pH ~ 4 (Figure 2) and ATMP at pH ~ 7 (Figure 3).

Table 1. Difference between calcium ion concentration at the beginning and end of the gypsum crystallization process (after 240 minutes) in the presence and absence of inhibitors at different pH values.[34]

	Additive -free	HEDP- pH ~ 4	HEDP- pH ~ 7	ATMP- pH ~ 4	ATMP- pH ~ 7	PAPEMP- pH ~ 4	DTPMPA- pH ~ 4	BHMTPMPA - pH ~ 4
$\Delta_{Ca^{2+}}$(mM)	72 ± 1.4	69 ± 1.3	59 ± 1.2	58± 1	0	48 ± 0.9	42 ± 0.8	0

To shed light on the role of these phosphorous containing additives in inhibiting gypsum crystallization, the amount of inhibitors taken up by the as-produced and desorbed gypsum crystals was quantified (Figure 6). For the as-formed crystals at pH ~ 4, the amount of inhibitor associated with the solid crystals ($C_{A,inhibitor}$) was lowest for the HEDP system (below the detection limit of our analytical method (ICP-OES)), and highest for the ATMP system with a $C_{A,inhibitor}$ of ~ 0.0013. In the PAPEMP and DTPMPA systems the $C_{A,inhibitor}$ was ~ 40 % and ~ 45 % lower than that for the ATMP additive, respectively. For the as-formed crystals at pH ~ 7, the highest $C_{A,inhibitor}$ value (~ 0.0015) was found for the HEDP system; this was also the highest uptake amount overall. After desorption, our data revealed that only ~ 10 % of the additives were desorbed, while ~ 90 % of the associated inhibitors remained associated with the as-formed gypsum crystals.[34]

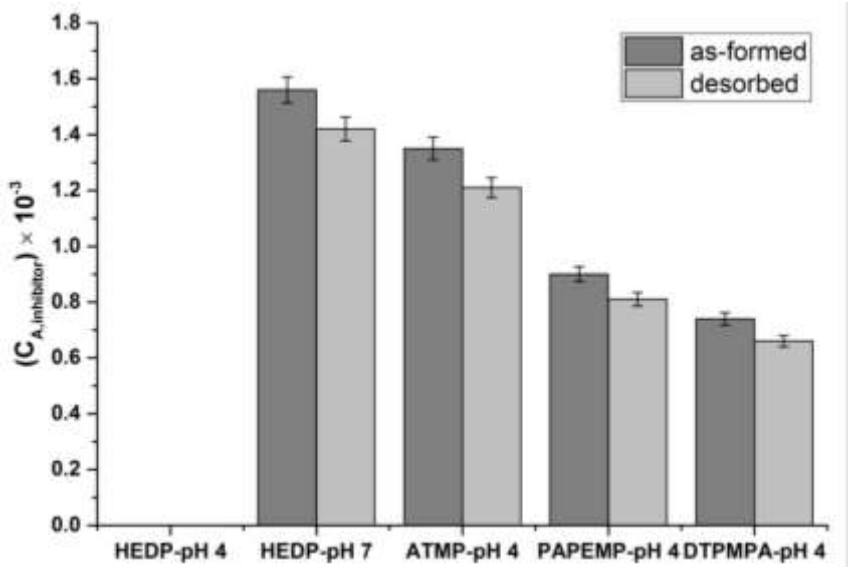

Figure 6. Inhibitors' association with end-product gypsum crystals in the presence of 20 ppm HEDP, ATMP, PAPEMP and DTPMPA at pH ~ 4 or ~ 7. Note that no gypsum crystals were obtained in the BHMTMPMA amended experiments (see Figure 1).[34]

The topmost surface layers of the produced crystals synthesised with 20 ppm phosphonate inhibitors were probed by XPS (Table 2). The atomic composition data show that except in the HEDP- pH ~ 4 and HEDP- pH ~ 7 systems, phosphorous was detected on the surface of the gypsum crystals precipitated in the presence of ATMP, PAPEMP and DTPMPA at pH ~ 4.

As an example the XPS spectra for DTPMPA at pH ~ 4 is shown in Figure 7. Besides Ca 2p (12.6 at.%), S 2p (12.8 at.%) and O 1s (58.9 at.%) with binding energies at 346.98 eV, 167.98 eV, and 530.98 eV, corresponding to gypsum, the XPS spectra also revealed the presence of Na 1s (0.2 at.%), Cl 2p (0.2 at.%), P 2p (0.9 at.%), and N 1s (0.3 at. %) at binding energies of 1072 eV, 193 eV, 133.4 eV, and 399.98 eV respectively. The Na and Cl spectral signatures are related to the presence of NaCl, in the crystallization solution whilst P and N signals correspond to the DTPMPA antiscalant. It is also worth noting that after desorption experiments neither P nor N was detected on the surface of the precipitated crystals.

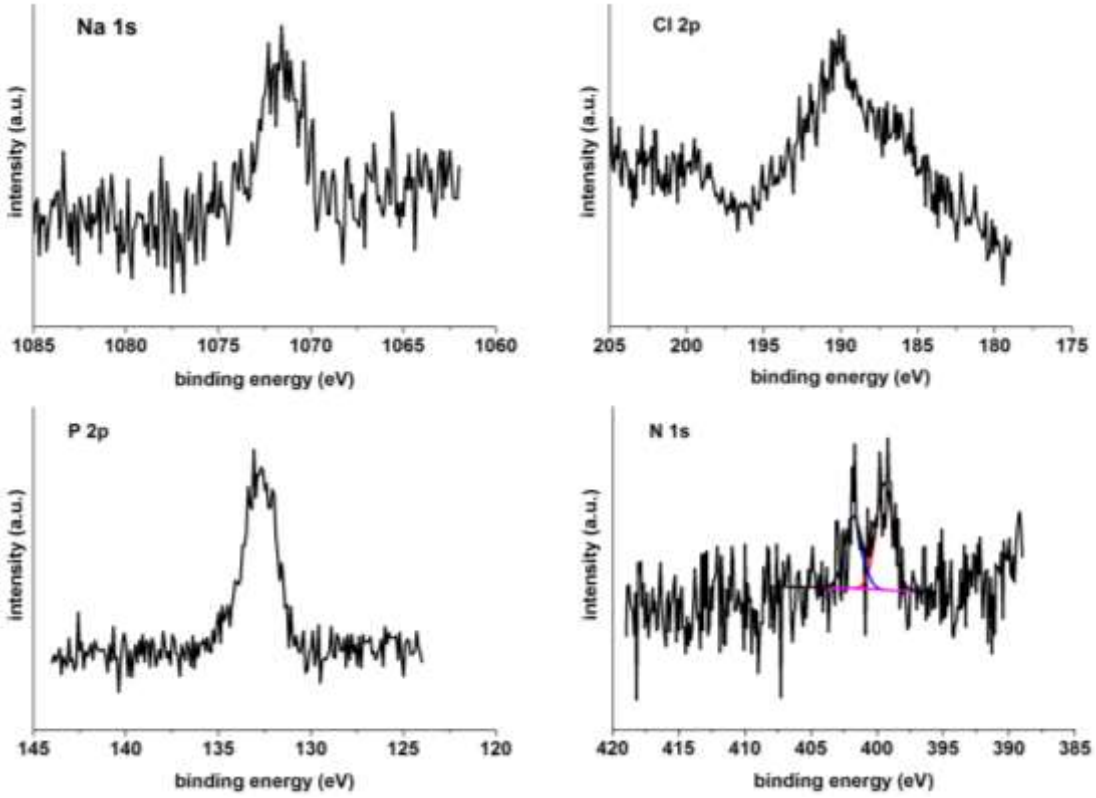

Figure 7. XPS spectra for the as-formed gypsum crystals precipitated in the presence of 20 ppm DTPMPA at pH ~ 4. Note that the peak intensities are in arbitrary units and do not represent the concentration of the elements on the surface.[34]

Table 2. Surface composition of the precipitated gypsum crystals detected by XPS (at. %); note that no gypsum crystals precipitated from a solution containing 20 ppm BHMTPMPA at pH ~ 4. In addition, in all systems no P and N was detected after desorption experiments

	Ca	S	O	Na	Cl	P	N	C[1]
Additive-free	11.8	12.1	61.2	0.2	-	-	-	14.7
HEDP-pH ~ 4	12.5	12.8	58.6	0.2	-	-	-	15.9
HEDP-pH ~ 7	12.4	12.8	59.6	0.2	0.1	-	-	14.9
ATMP-pH ~ 4	12.3	12.8	59.6	0.5	0.1	0.5	-	14.2
ATMP-pH ~ 4 (after desorption)	12.6	12.9	59.6	-	0.2	-	-	14.7
PAPEMP-pH ~ 4	12.2	12.7	58.5	0.3	0.2	0.2	-	15.6
DTPMPA-pH ~ 4	12.6	12.8	58.9	0.2	0.2	0.9	0.3	14.3

1 adventitious carbon

The morphology of the gypsum crystals grown from supersaturated solutions with or without additives were characterised by SEM (Figure 8). In the absence of inhibitors almost exclusively large and thin twin crystals were produced (Figure 8 a). This was similar to the crystals formed in the presence of HEDP at pH ~ 4 (Figure 8 b). However, both HEDP at pH ~ 7 (Figure 8 c) and ATMP at pH ~ 4 (Figure 8 d) dramatically modified the morphology of the gypsum crystals resulting in thick needle shaped particles. The other additives, PAPEMP and DTPMPA, also had profound effects on the morphology and sizes of the formed gypsum crystals. PAPEMP at pH ~ 4 yielding a mixture of long "dendritic" needles with thick short crystals (Figure 8 e), and DTPMPA at pH ~ 4 resulted in thick and short crystals together with some long dendritic crystals covered by tiny crystal fragments (Figure 8 f).[34]

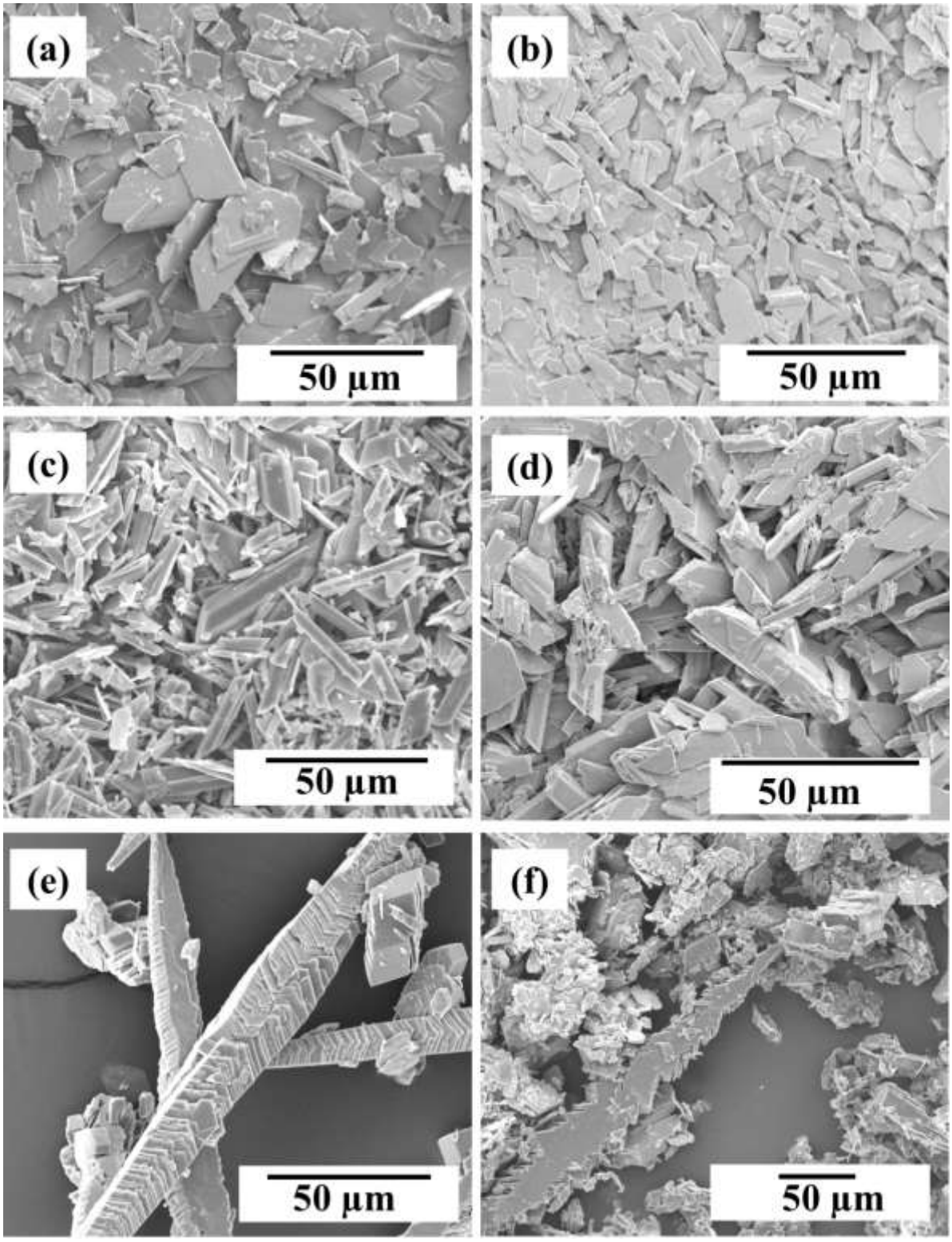

Figure 8. SEM micrograph of gypsum crystals gathered after 240 minutes from experiments in (a) additive-free at pH ~ 7; (b) 20 ppm HEDP at pH ~ 4; (c) 20 ppm HEDP at pH ~ 7; (d) 20 ppm ATMP at pH ~ 4; (e) 20 ppm PAPEMP at pH ~ 4; (f) 20 ppm DTPMPA at pH ~ 4; note that no gypsum crystals precipitated from a solution containing 20 ppm BHMTPMPA at pH ~ 4.[34]

4. Discussion

4.1. Crystallization kinetics: role of additives

We used the change in induction times from the turbidity curves derived from the gypsum precipitation experiments carried out without and with phosphonate antiscalants to study the effects they have on crystallization of calcium sulfate dihydrate. Our measurements at pH ~ 4 revealed a remarkable increase in induction time and a decrease in nucleation and growth kinetics in the presence of 20 ppm additives following the order HEDP < ATMP < PAPEMP < DTPMPA < BHMTPMPA (Figure 2).

The observed turbidity graphs in this research differ from those plotted in our previous studies[39,40], where other, non-phosphonate containing, antiscalants were used to retard gypsum formation. This is probably due to the specific physico-chemical properties of the phosphonate-containing antiscalants, which control the mechanisms by which these additives interact with gypsum crystals, in particular those properties that are thought to be among the main factors affecting the performance and efficiency of antiscalants, such as molecular structure, presence of functional groups, and molecular weight of antiscalants together with the pH of the solution.[1,41] It is also well-known that scaling inhibitors can decrease the formation of undesirable minerals by different mechanisms, such as through ion sequestration or chelation, increasing the interfacial tension between nuclei and the crystallization solution, dispersing the scale minerals, and / or association with the crystal (e.g., surface adsorption).[42,43] Even among the phosphonate additives, differences in their physico-chemical properties yielded different turbidity development trends (Figure 2, 3). For example, the turbidity graphs in the experiments with HEDP and ATMP at pH ~ 4 were similar to each other but markedly different than those in experiments with PAPEMP, DTPMPA at pH ~ 4 and HEDP at pH ~ 7. Furthermore, in the presence of PAPEMP at pH ~ 4 (Figure 2), the turbidity development changed ~ 65 minutes after induction (at ~ 30 %

turbidity) and switched to increase but with a lower slope which may originate from the changes in the interaction of PAPEMP with gypsum crystals over time.[34]

Some of the mechanisms thought to control the interaction of additives with mineral crystals in relation to our phosphonate data are discussed below.

4.1.1. Sequestration or chelation: Phosphonate antiscalants are known to retard crystallization by chelating with active ions in the precipitation solutions.[44] In our case, complexation with Ca^{2+} ions would result in a decrease in the activity of free Ca^{2+} and $CaSO_4^0$ ion pairs, which is likely reflected by the delay in gypsum crystallization kinetics (Figures 2, 3 and 5). The role of pH is also fundamental in chelation ability of the phosphonate inhibitors because these compounds deprotonate at higher pH and further complex with Ca^{2+}, and therefore hinder the crystallization which was also demonstrated in this study (Figure 5).[34] Table 1 further illustrates the chelation performance of the studied inhibitors and reveals the strong complexation between the phosphonate functional groups and Ca^{2+} especially at higher pH values. The sequestrating ability of phosphonates towards cations has also been demonstrated.[45] Variations in total calcium *vs.* time plots in the absence and presence of phosphonate antiscalants may also further illustrate the positive effects of the tested additives on the gypsum formation rate.

4.1.2. Molecular structure: We note that there is a direct relation between the number of functional groups in the phosphonate inhibitor structure and the decrease in gypsum crystallization kinetics (Figure 2). In this regard, it is likely that DTPMPA and BHMTPMPA each with five phosphonate functional groups more effectively complexed with Ca^{2+} than PAPEMP, ATMP and HEDP with four, three and two functional groups, respectively, (Table 1) and thus more effectively inhibited gypsum crystallization (i.e., DTPMPA and BHMTPMPA showed the longest induction times; Figure 2). A more effective inhibition of calcite crystallization by the five phosphonate functional group DTPMPA

316 compared to the tetraphosphonate inhibitors is also reported elsewhere and similarly
317 attributed to a more effective complexation of phosphonate functional groups of
318 DTPMPA.[46,34] However, Zhang el al.[47], reported the higher $CaCO_3$ formation inhibition
319 efficiency of PAPEMP than DTPMPA.

320 In terms of molecular length, we observed here that at constant concentration of 20
321 ppm (29.2 µM) BHMTPMPA, no changes in turbidity was detected, indicating an even
322 higher inhibitory efficiency of this additive than 20 ppm (34.9 µM) DTPMPA (Figure 2).
323 Although the pK values for DTPMPA and BHMTPMPA have not yet been determined,
324 assuming very close pK values for DTPMPA and BHMTPMPA, we suggest that the
325 differences in inhibitory efficiency are related to differences in the molecular structure of
326 these two antiscalants, i.e. the backbone chain length where DTPMPA and BHMTPMPA
327 contain 4 and 12 methylene groups in their backbone connecting the N atoms, respectively.
328 Akyol et al.,[48] showed that a tetraphosphonate antiscalant with a longer backbone chain had a
329 greater gypsum inhibitory efficiency than tetraphosphonate antiscalants with shorter
330 backbone chains and as such we also attribute the greater inhibitory efficiency of
331 BHMTPMPA compared to DTPMPA to this molecular structure effect. Recent work by Shi
332 et al.,[49] focused on this molecular structure phenomenon and used a molecular modelling
333 approach to show that there is an optimum PAPEMP molecular length for increased
334 anhydrite inhibition and among the PAPEMP antiscalants with different methylene groups (n
335 = 1-7), the PAPEMP with 3 methylene groups had higher adsorption on calcium sulfate
336 anhydrite. The Shi et al. results, however, are contrary to similar molecular modelling for
337 calcite which showed that because of steric hindrance effects, the tetraphosphonate inhibitors
338 with longer back bone chains resulted in a weaker inhibition of calcite crystallization.[49,34]

339 It is also worth noting that the molar concentration of BHMTPMPA added to the
340 crystallization solution (i.e., 29.2 μM) was about 3 times lower than that of for HEDP (i.e.,
341 97.1 μM). This further illustrates the profound effect of molecular structure of an antiscalant.
342 **4.1.3. Surface adsorption / structural incorporation:** It was shown in this research
343 that the deprotonation state of the additives in the crystallization solutions can directly affect
344 the concentration variation of the additives during the crystallization experiments, and the
345 association of the additives with the forming gypsum crystals (Figures 4-6).[34]
346 It is well-known that antiscalants with deprotonated functional groups adsorb onto
347 developing nuclei and / or growing crystals by binding onto active growth sites (i.e., steps
348 and kink sites). During this process just a few percent of a crystal surface (e.g., 5 % in the
349 barite system) needs to be covered to totally block crystal growth.[50] Adsorption of inhibitors
350 also affects the thermodynamic stability of nuclei by keeping them at subcritical size and
351 dissolving the nuclei before their further growth. Then, the inhibitors are available for
352 repeated adsorption.[51] It is also worth mentioning that beside surface binding, impurities can
353 trap within the growing gypsum crystal structure and association of foreign ions with gypsum
354 crystals increases with increasing crystal growth rate.[52,34]
355 Here, HEDP at pH ~ 4 is weakly deprotonated and therefore it is likely that this
356 additive did not adsorb on the gypsum crystal surfaces and did not become trapped in the
357 rapidly growing gypsum crystals (Figure 2 and 4). This is evident in the fact that the HEDP
358 concentration did not decrease during the experiment (Figure 4). Overall, with no HEDP
359 association with the gypsum crystals there was no gypsum inhibition (Figure 2). In contrast,
360 HEDP at pH ~ 7 and ATMP at pH ~ 4 were deprotonated and therefore likely adsorbed and
361 became trapped in the fast growing gypsum crystals, which caused a significant decrease in
362 HEDP and ATMP concentration during the crystallization process (Figures 2, 4 and 5).[34]

We also observed that besides the degree of deprotonation, the amount of the precipitated crystals (degree of turbidity) affects the concentration of the inhibitors in the solution. According to Figure 5, in HEDP system at pH ~ 7, an abrupt increase in turbidity occurred when it reached ~ 3 %. This could be due to the depletion of HEDP from the crystallization solution because of the association of the inhibitors with the nucleating and growing gypsum crystals. HEDP at pH ~ 7 and ATMP at pH ~ 4 were not strong inhibitors to fully sequestrate the Ca^{2+} in the solution and prevent the gypsum formation. Therefore, by precipitating more crystals and increasing the turbidity in the mixing solution with time, the phosphonate functional groups further associated with gypsum and therefore their concentration gradually decreases in the solution. In the case of HEDP at pH ~ 7, this continued over time until at a certain point (~ 3 % in the case of HEDP at ~ 7) where in the absence of the deprotonated inhibitors, gypsum crystals easily precipitated, as mirrored by the sharp increase in the turbidity with a slope very close to the phosphonate-free system (Figure 5) resulted in a high association amount measured by ICP analysis (Figure 6). A similar trend in turbidity development was observed when 20 ppm polyacrylic acid was added to gypsum crystallization solution.[53]

In PAPEMP and DTPMPA systems at pH ~ 4, due to highly Ca^{2+} sequestration, less amount of gypsum crystals nucleated and their growth were significantly hindered. Thus, more than 50 % of these additives remained in the crystallization solution after 240 minutes. Therefore, low association amount was measured for these two systems (Figure 6).

To shed light on the surface adsorption *vs.* structural incorporation of our additives with gypsum, we performed desorption experiments and used a combination of ICP-OES analysis of digested as-formed and post-desorbed gypsum crystals, together with XPS studies of the surfaces of these solids (Figure 6 and Table 2). Evaluating the association of additives with gypsum crystals after 2 hours of desorption, ICP-OES revealed that just ~ 10 % of

388 associated inhibitors desorbed and thus a the majority (~ 90 %) remained associated with the
389 solid crystals, which could be due to (i) strong surface binding (i.e., adsorption) and thus no
390 desorption and / or (ii) incorporation into the crystal structure (i.e., structural incorporation)
391 and thus no desorption (Figure 6).

392 (i) In the case of a strong surface binding mechanism: it is well-known that the
393 surface charge of the adsorbent (here gypsum) and the nature of the adsorbate (e.g.,
394 phosphonate additives) affect the extent of adsorption. Calcium ions in the gypsum structure
395 have high hydration energy therefore they are highly shielded by the mineral structural water
396 molecules and those of the surrounding solution.[54,34] A negative surface charge for gypsum at
397 pH values above ~ 2 has also been reported.[55] Therefore, this implies that phosphonate
398 functional groups did not adsorb onto the crystals via physisorption (electrostatic interaction)
399 but their adsorption was via an irreversible chemisorption mechanism called "specific
400 adsorption" (also called "ligand-exchange" or "coordination adsorption") during which the
401 hydroxyl groups linked to the calcium ions are replace by the phosphonate additives.[56] The
402 adsorption of anions onto hydrated minerals (e.g., α-alumina[57]) via a ligand exchange
403 mechanism has also been documented. Similarly to this study, Weijnen and Van Rosmalen[58]
404 observed the association of HEDP with negatively surface charged gypsum crystals and did
405 not measure any desorbed HEDP even after several days suspending the gypsum crystals in a
406 supersaturated gypsum solution. These authors, therefore, suggested that the strong
407 association of HEDP with gypsum is irreversible but they did not distinguish whether the
408 irreversibility was due to the strong "ligand exchange" adsorption or structural incorporation.
409 The structural incorporation of HEDP into hydroxyapatite at high temperature and after long
410 reaction times has also been reported.[59] Furthermore, Akyol et al.[48] proposed that negatively
411 charged phosphonates bind to the calcium ions of the gypsum structure by substituting the
412 water molecules of the hydrated calcium ions in a process called "calcium-phosphonate

413 interaction". Indeed, precipitation of a calcium-phosphonate layer on calcium based cement
414 grains in the presence of ATMP has been similarly proposed[60,34], and the formation of
415 calcium phosphonate compounds (Ca-DTPMPA) on calcite surfaces have also been
416 identified.[61]

417 (ii) Assuming a structutral incorporation mechanism, we suggest that for structural
418 incorporation of the studied inhibitors, at first the additives should strongly adsorb onto the
419 gypsum crystals and then they become trapped during gypsum growth. In the HEDP system
420 at pH ~ 4 no surface adsorption or structural incorporation was observed (Figure 6), but at pH
421 ~ 7 we measured P by ICP-OES in digested as-formed gypsum crystals, but the XPS analysis
422 did not detect any P on the surface of those crystals, suggesting that the HEDP was
423 incorporated into the structure of the crystals away from the structural surface (Figure 6 and
424 Table 1).

425 In ATMP system at pH ~ 4, the P XPS peak vanished after desorption experiments
426 suggesting that all of the ATMP was removed from the surface of the crystals, but ICP-OES
427 analysis measured the P in the digestion solution of post-desorption crystals, again suggesting
428 the structural incorporation of ATMP (Table 2).

429 It is also worth mentioning that XPS analysis of as-formed gypsum crystals
430 precipitated from 20 ppm DTPMPA amended solution at pH ~ 4, revealed that in acidic
431 solutions, nitrogen atoms of amino groups in DTPMPA can be protonated and adsorb to the
432 negatively charged sites of a gypsum crystal (Figure 7). This was previously shown for a
433 mirabilite crystal.[62,63] Therefore, the N 1s peak with two components located at binding
434 energies of 399.4 eV and 401.7 eV has been assigned to amino groups and protonated
435 nitrogen (NH^{3+}) on the gypsum surface, respectively.[64]

436

437 **4.3. Morphological modification**

As our morphological investigations show, selective adsorption and structural incorporation of phosphonates onto and into the growing crystals inhibited their growth along specific directions and thus changed their morphology (Figure 8). This is a common phenomenon, but our imaging data confirmed that with phosphonate additives, gypsum crystals change their habits compared to those in the additive-free system. It is also worth mentioning that the irregular twinned morphology of the gypsum crystals without and with additives in this study was different to the needle shape morphology of the additive-free gypsum crystals reported in our previous studies.[39,40] This could be due to the higher supersaturation of the gypsum crystallization solution (0. 84 *vs.* 0.55) and the larger volume of the crystallization solution (1 litre *vs.* 2 ml) in this study, but further investigation of the effects of the supersaturation and the solution volume on gypsum crystallization were out of the scope of this study. Other studies using HEDP and ATMP also showed that as a function of supersaturations the morphology of the forming gypsum crystals changes.[65,34]

HEDP at pH ~ 4 was likely not deprotonated enough to interact with the growing gypsum crystals and so did not associate and therefore did not cause any morphological changes (Figure 8 b). On the other hand, HEDP at pH ~ 7 yielded gypsum crystals with different morphologies (Figure 8 c). This additive at pH ~ 7 inhibited the growth along the *c* axis and favoured the growth of gypsum in the *a* and *b* directions, leading to dominantly thick crystal habits instead of thin twin crystals. This morphological change was further demonstrated by changes in XRD peak intensity ratios where the (020) to (021) peak intensity ratio in the HEDP amended system at pH ~ 7 was smaller (~ 0.69) than the corresponding ratio at pH ~ 4 (~ 2.6) (Figure 9). Considering the typical gypsum unit cell[66], this variation in peak intensity ratio is attributed to the increase in thickness of the crystal accompanied by an increase in (021) peak intensity. A similar change in XRD peak intensity

ratio, and associated morphological changes, as a result of a carboxylic acid adsorption onto another calcium sulfate phase (bassanite; $CaSO_4 \cdot 0.5H_2O$) has been reported.[67,34]

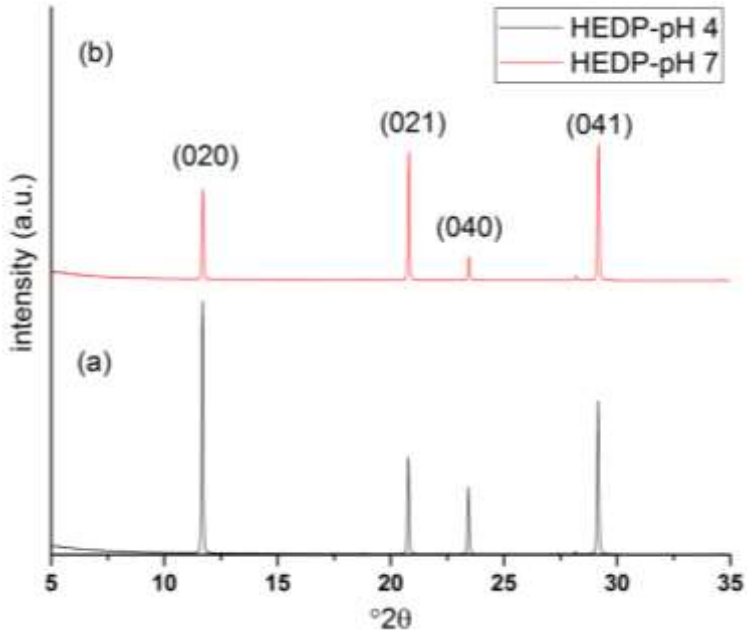

Figure 9. The effects of HEDP on gypsum (020) to (021) peak intensity ratio at two different pH values of (a) ~ 4 and (b) ~ 7.[34]

In terms of the other additives, thicker needle gypsum crystals were also observed as a consequence of ATMP association at pH ~ 4 (Figure 8 d), while stronger association of PAPEMP and DTPMPA containing four and five phosphonate functional groups at pH ~ 4 yielded gypsum crystals that were shorter and thicker (Figure 8 e,f).[34]

In addition, the tips of the gypsum crystals obtained from in the absence of additives had dominantly flat tips but in the presence of 20 ppm HEDP pH ~ 7 and ATMP, PAPEMP and DTPMPA pH ~ 4, the macro-steps on the broader and thicker gypsum crystals were also obvious (Figure 10). The observed macro-steps for the crystals grown in the presence of phosphonates, together with uneven crystal tips and the presence of growth steps on the crystal surfaces further confirm the adsorption of inhibitors on the gypsum crystals. Similarly,

the presence of growth steps has been observed for gypsum crystals grown with acrylic polymers.[68]

However, PAPEMP and DTPMPA at pH ~ 4 produced long dendritic gypsum crystals as well. Here, we emphasise due to the lack of SEM images from forming gypsum crystals during turbidity development process in both PAPEMP and DTPMPA at pH ~ 4 systems, it is not possible to determine at what turbidity development step these two morphologies (i.e.,"short, thick" and "long, dendritic") precipitated. But, formation of long dendritic gypsum crystals can probably be related to the long molecular structure of PAPEMP and DTPMPA.[34] According to the models proposed by Barouda et al.,[69] and Akyol et al.,[48] these long molecules are flexible and can bend which may allow these additives to interact with calcium and / or sulfate ions in different crystal faces yielding long "dendritic" crystals. However, a detailed molecular level understanding of the process is still outstanding.

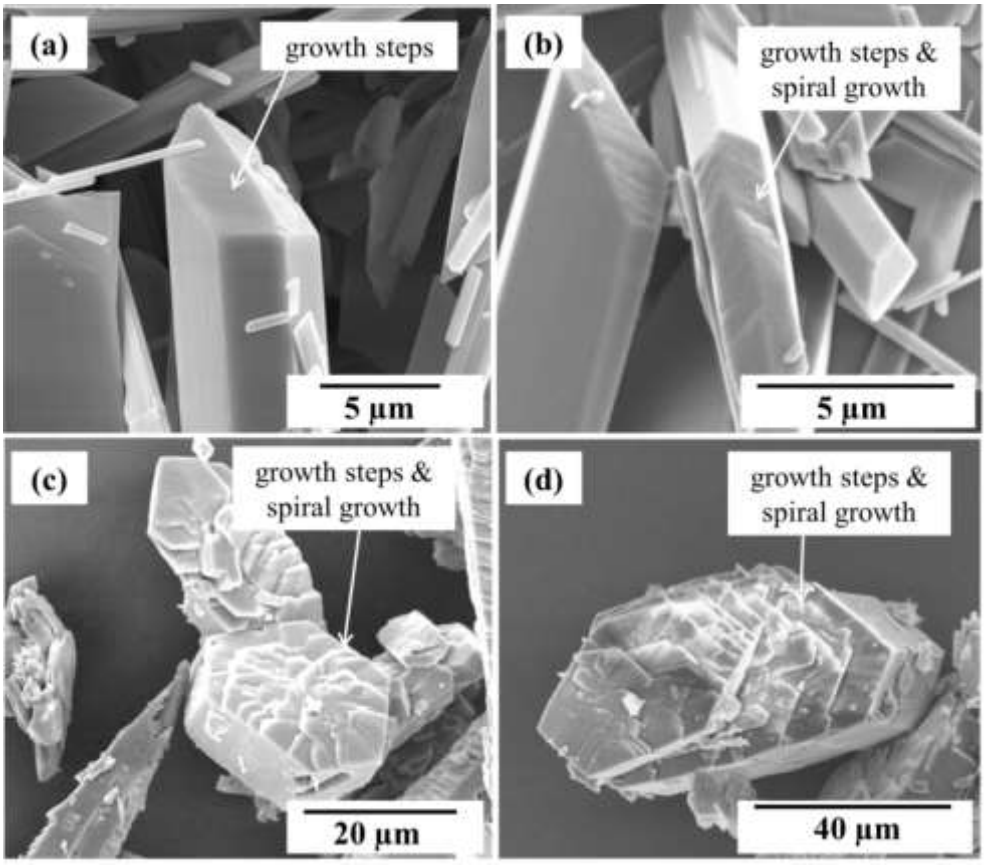

Figure 10. The spiral growth and macro-steps on the broader and thicker gypsum crystals gathered after 240 minutes from experiments in (a) 20 ppm HEDP at pH ~ 7; (b) 20 ppm ATMP at pH ~ 4; (c) 20 ppm PAPEMP at pH ~ 4; (d) 20 ppm DTPMPA at pH ~ 4.

Considering the efficiency of the tested inhibitors and the morphology of precipitated gypsum crystals, BHMTMPA is the most suitable phosphonate inhibitor to be used in different industries. Moreover, we emphasise that the phosphonate additives should be added at high enough concentration (e.g., ~ 20 ppm) to the gypsum crystallization solution to prevent the gypsum formation, otherwise after the depletion of antiscalant from the solution, thick and long dendritic needle crystals will form which might clog pipelines and membranes and cause problems in some industries such as reverse osmosis water desalination, etc.[34]

Although in this paper the mechanisms by which phoshponate antiscalants hinder gypsum formation were investigated, to decrease the environmental impacts of these additives, we also highlight the importance of using biodegradable additives such as polyepoxysuccinic acid and polyaspartic acid in preventing gypsum formation.[53]

5. Conclusion

In this research, we reported the effects of industrial phosphonate containing additives on the crystallization kinetics of gypsum mineral. The presence of additives led to inhibition of gypsum formation because they increased the time needed for gypsum precipitation in the order of increasing number of phosphonate functional groups in the antiscalant additive as follows: HEDP < ATMP < PAPEMP < DTPMPA < BHMTPMPA. Gypsum was the only mineral phase after 240 minutes and no phase transformation was recorded in the presence of the additives. Combination of ICP-OES and XPS analyses revealed that highly deprotonated antiscalants associated with gypsum crystals through surface adsorption and / or structural incorporation. This was accompanied by a decrease in the additive's concentration in the

crystallization solution during gypsum growth. Just ~ 10 % of the associated additives were adsorbed to the surface while the remainder was either strongly adsorbed or structurally incorporated. Growing in the presence of additives affected the morphology of the gypsum crystals. Thin and twin gypsum crystals precipitated from additive-free solutions compared to short and thick crystals in the presence of HEDP at pH ~ 7 and ATMP at pH ~ 4. This was in contrast to gypsum growth in the presence of PAPEMP and DTPMPA at pH ~ 4, where short and thick crystals and long dendritic needles were obtained.

Acknowledgement

This study was supported by a Marie Curie grant from the European Commission in the framework of the MINSC ITN (Initial Training Research network), Project number 290040.

References

(1) MacAdam J., Jarvis, P., Water-Formed Scales and Deposits: Types, Characteristics, and Relevant Industries. In *Mineral Scales and Deposits: Scientific and Technological Approaches,* 1st ed.; Z. Amjad and K. D. Demadis eds, Elsevier, Amsterdam, 2015, pp 3-47.

(2) Huber, P.; Nivelon, S.; Ottenio, P; Nortier, P. Coupling a Chemical Reaction Engine With a Mass Flow Balance Process Simulation for Scaling Management in Papermaking Process Waters, *Ind. Eng. Chem. Res.* **2012,** *52,* 421-429.

(3) Javanmard, H.; Seyyedi, M.; Nielsen, S.M. On Oil Recovery Mechanisms and Potential of DME–Brine Injection in the North Sea Chalk Oil Reservoirs. *Ind. Eng. Chem. Res.* **2018,** *57,* 15898-15908.

(4) Supekar, O.D.; Brown, J.J.; Greenberg, A.R.; Gopinath, J.T.; Bright, V.M. Real-Time Detection of Reverse-Osmosis Membrane Scaling via Raman Spectroscopy. *Ind. Eng. Chem. Res.* **2018,** *57,* 16021-16026.

(5) Liu, W.; Chien, S.H.; Dzombak, D.A.; Vidic, R.D. Scaling Control for Heat Exchangers in Recirculating Cooling Systems Using Treated Municipal Wastewater. *Ind. Eng. Chem. Res.* **2014,** *53,* 16366-16373.

(6) Davoody, M.; Graham, L.J.; Wu, J.; Youn, I.; Abdul Raman, A.A.; Parthasarathy, R. A. Novel Approach To Quantify Scale Thickness and Distribution in Stirred Vessels. *Ind. Eng. Chem. Res.* **2017,** *56,* 14582-14591.

(7) Kim, M.M.; Au, J.; Rahardianto, A.; Glater, J.; Cohen, Y.; Gerringer, F.W.; Gabelich, C.J. Impact of Conventional Water Treatment Coagulants on Mineral Scaling in RO Desalting of Brackish Water. *Ind. Eng. Chem. Res.* **2009,** *48,* 3126-3135.

(8) Li, J.; Zhou, Y.; Yao, Q.; Wang, T.; Zhang, A.; Chen, Y.; Wu, W.; Sun, W. Preparation and Evaluation of a Polyether-Based Polycarboxylate as a Kind of Inhibitor for Water Systems. *Ind. Eng. Chem. Res.* **2017,** *56,* 2624-2633.

(9) Kelland, M.A. Effect of Various Cations on the Formation of Calcium Carbonate and Barium Sulfate Scale With and Without Scale Inhibitors. *Ind. Eng. Chem. Res*. **2011**, *50*, 5852-5861.

(10) Johnson, M.; Peakall, J.; Fairweather, M.; Biggs, S.; Harbottle, D.; Hunter, T.N. Characterization of Multiple Hindered Settling Regimes in Aggregated Mineral Suspensions. *Ind. Eng. Chem. Res.* **2016,** *55,* 9983-9993.

(11) Maffra, D.A.; Freitas, T.C.; da Cruz, G.F.; de Siqueira, F.D.; do Rosário, F.F. Evaluation of Barium Sulfate Scale Inhibition Using Relative Permeability Modifier Polymers as Adsorption Enhancer for Mature Offshore Well Treatments in Campos Basin, Brazil. *Ind. Eng. Chem. Res.* **2018,** *57,* 11493-11504.

568 (12) Al-Hamzah, A.A.; Smith, E.J.; Fellows, C.M. Inhibition of Homogeneous Formation of
569 Magnesium Hydroxide by Low-Molar-Mass Poly (Acrylic Acid) With Different End-
570 Groups. *Ind. Eng. Chem. Res.* **2015,** *54,* 2201-2207.
571 (13) Demadis, K.D.; Mavredaki, E; Somara, M. Additive-Driven Dissolution Enhancement of
572 Colloidal Silica. 2. Environmentally Friendly Additives and Natural Products. *Ind.*
573 *Eng. Chem. Res*. **2011**, *50*, 13866-13876.
574 (14) Gilron, J.; Ladizansky, Y.; Korin, E. Silica Fouling in Direct Contact Membrane
575 Distillation. *Ind. Eng. Chem. Res*. **2013,** *52,* 10521-10529.
576 (15) Halevy, S.; Korin, E.; Gilron, J. Kinetics of Gypsum Precipitation for Designing
577 Interstage Crystallizers for Concentrate in High Recovery Reverse Osmosis. *Ind. Eng.*
578 *Chem. Res*. **2013,** *52,* 14647-14657.
579 (16) Wang, W.; Zeng, D.; Wang, J.; Li, H.; Wu, L. Experimental Determination and
580 Modeling of the Solubility of $CaSO_4 \cdot 2H_2O$ and $CaSO_4$ in the Quaternary System
581 $CaSO_4 + MgSO_4 + H_2SO_4 + H_2O$. *Ind. Eng. Chem. Res*. **2014,** *53,* 12839-12847.
582 (17) Freyer, D.; Voigt, W. Crystallization and Phase Stability of $CaSO_4$ and $CaSO_4$ - Based
583 Salts. *Monatshefte fur Chemie / Chemical Monthly* **2003,** *134*, 693-719.
584 (18) Adams, J. F.; Papangelakis, V. G. Gypsum Scale Formation in Continuous
585 Neutralization Reactors, *Can. Metall. Q.* **2000,** *39*, 421-432.
586 (19) Crabtree, M.; Eslinger, D.; Fletcher, P.; Miller, M.; Johnson, A.; King, G. Fighting
587 Scale—Removal and Prevention, *Oilfield Rev.* **1999,** *11*, 30-45.
588 (20) Kelland, M. A. Production Chemicals for the Oil and Gas Industry. 2nd ed.; CRC press;
589 New York 2014; pp 51-111.
590 (21) Piyadasa, C.; Ridgway, H. F.; Yeager, T. R.; Stewart, M. B.; Pelekani, C.; Gray, S. R.;
591 Orbell, J. D. The Application of Electromagnetic Fields to the Control of the Scaling

592 and Biofouling of Reverse Osmosis Membranes-A Review. *Desalination* **2017,** *418*,
593 19-34.
594 (22) Olajire, A. A. A Review of Oilfield Scale Management Technology for Oil and Gas
595 Production. *J. Pet. Sci. Eng.* **2015,** *135*, 723-737.
596 (23) Hasson, D.; Shemer, H.; Sher, A. State of the Art of Friendly "Green" Scale Control
597 Inhibitors: A Review Article. *Ind. Eng. Chem. Res.* **2011,** *50*, 7601-7607.
598 (24) Ketrane, R.; Saidani, B.; Gil, O.; Leleyter, L.; Baraud, F. Efficiency of Five Scale
599 Inhibitors on Calcium Carbonate Precipitation From Hard Water: Effect of
600 Temperature and Concentration. *Desalination* **2009,** *249*, 1397-1404.
601 (25) Abd-El-Khalek, D.; Abd-El-Nabey, B. Evaluation of Sodium Hexametaphosphate as
602 Scale and Corrosion Inhibitor in Cooling Water Using Electrochemical Techniques.
603 *Desalination* **2013,** *311*, 227-233.
604 (26) Li, J.; Zhou, Y.; Yao, Q.; Wang, T.; Zhang, A.; Chen, Y.; Wu, W.; Sun, W. Preparation
605 and Evaluation of a Polyether-Based Polycarboxylate as a Kind of Inhibitor for Water
606 Systems. *Ind. Eng. Chem. Res*. **2017**, *56*, 2624.
607 (27) Al-Hamzah, A.A.; Wallace, A.D.; East, C.P.; Doherty, W.O.; Smith, E.J.; Fellows, C.M.
608 Inhibition by Poly (Acrylic Acid) and Morphological Changes in Calcium Carbonate
609 and Calcium Carbonate/Calcium Sulfate Crystallization on Silica Fibers. *Ind. Eng.*
610 *Chem. Res*. **2014,** *53,* 8793-8803.
611 (28) Prisciandaro, M.; Olivieri, E.; Lancia, A.; Musmarra, D. Gypsum Precipitation from an
612 Aqueous Solution in the Presence of Nitrilotrimethylenephosphonic Acid. *Ind. Eng.*
613 *Chem. Res.* **2006,** *45*, 2070-2076.
614 (29) Ojo, S. A.; Slater, B.; Catlow, C. Computer Simulation of Calcite Growth Inhibition: A
615 Study of Monophosphonate Interaction With Calcite. *Mol. Simulat.* **2002,** *28*, 591-
616 606.

(30) Nygren, M. A.; Gay, D. H.; Catlow, C. R. A.; Wilson, M. P.; Rohl, A. L. Incorporation of Growth-Inhibiting Diphosphonates Into Steps on the Calcite Cleavage Plane Surface. *J. Chem. Soci., Faraday Trans.* **1998,** *94*, 3685-3693.

(31) Mavredaki, E.; Neville, A.; Sorbie, K. S. Initial Stages of Barium Sulfate Formation at Surfaces in the Presence of Inhibitors. *Cryst. Growth Des.* **2011,** *11*, 4751-4758.

(32) Sousa, M. F.; Bertran, C. A. New Methodology Based on Static Light Scattering Measurements for Evaluation of Inhibitors for in Bulk $CaCO_3$ Crystallization. *J. Colloid Interface Sci.* **2014,** *420*, 57-64.

(33) Parkhurst D.L.; Appelo C.A.J. Description of Input and Examples for Phreeqc Version 3—a Computer Program for Speciation, Batch-Reaction, One-Dimensional Transport, and Inverse Geochemical Calculations: U.S. Geological Survey Techniques and Methods, vol. 6, ch.. A43, 497 p., available only at https://pubs.usgs.gov/tm/06/a43/.

(34) Rabizadeh, T. The Nucleation, Growth Kinetics and Mechanism of Sulfate Scale Minerals in the Presence and Absence of Additives as Inhibitors, PhD thesis, University of Leeds: Leeds, January 2017.

(35) Cooper, A. Biophysical Chemistry. 2nd ed. RSC publisher: Cambridge, 2011, p. 37.

(36) Sharma, B.K., Instrumental Methods of Chemical Analysis. 24th ed. Krishna Prakashan Media Ltd.: Meerut, 2005, p. 75.

(37) Jonasz, M.; Fournier, R. G., *Light Scattering by Particles in Water: Theoretical and Experimental Foundations*, chapter 3, Elsevier: London, 2011, p.p. 87-145.

(38) Tobler, D.J.; Blanco, J.R.; Dideriksen, K.; Sand, K.K.; Bovet, N.; Benning, L.G.; Stipp, S.L.S. The Effect of Aspartic Acid and Glycine on Amorphous Calcium Carbonate (Acc) Structure, Stability and Crystallization. *Procedia Earth Planet. Sci.*, **2014**, *10*, 143-148.

641 (39) Rabizadeh, T.; Peacock, C. L.; Benning, L. G. Carboxylic Acids: Effective Inhibitors for
642 Calcium Sulfate Precipitation?, *Mineral. Mag.* **2014,** *78*, 1465-1472.
643 (40) Rabizadeh, T.; Stawski, T. M.; Morgan, D. J.; Peacock, C. L.; Benning, L. G. The
644 Effects of Inorganic Additives on the Nucleation and Growth Kinetics of Calcium
645 Sulfate Dihydrate Crystals, *Cryst. Growth Des.* **2017,** *17*, 582-589.
646 (41) Guo, J.; Severtson, S.J. Inhibition of Calcium Carbonate Nucleation With
647 Aminophosphonates at High Temperature, pH and Ionic Strength. *Ind. Eng. Chem.*
648 *Res*. **2004,** *43,* 5411-5417.
649 (42) Lioliou, M. G.; Paraskeva, C. A.; Koutsoukos, P. G.; Payatakes, A. C. Calcium Sulfate
650 Precipitation in the Presence of Water-Soluble Polymers. *J. Colloid Interface Sci.*
651 **2006,** *303*, 164-70.
652 (43) Prisciandaro, M.; Olivieri, E.; Lancia, A.; Musmarra, D. PBTC as an Antiscalant for
653 Gypsum Precipitation: Interfacial Tension and Activation Energy Estimation. *Ind.*
654 *Eng. Chem. Res*. **2012,** *51,* 12844-12851.
655 (44) Gopi, S.P.; Subramanian, V.K.; Palanisamy, K. Synergistic Effect of EDTA and HEDP
656 on the Crystal Growth, Polymorphism, and Morphology of $CaCO_3$. *Ind. Eng. Chem.*
657 *Res*. **2015,** *54,* 3618-3625.
658 (45) Siek, M.; Kołodyńska, D.; Hubicki, Z. Sorption of Cd (II), Pb (II), Cu (II), and Zn (II)
659 Complexes with Nitrilotris (Methylenephosphonic) Acid on Polystyrene Anion
660 Exchangers. *Ind. Eng. Chem. Res*. **2010,** *49,* 4700-4709.
661 (46) Xia, M.; Chen, C. Probing the Inhibitory Mechanism of Calcite Precipitation by Organic
662 Phosphonates in Industrial Water Cooling System. *Int. J. Environ. Sci. Dev.* **2015,** *6*,
663 300-304.
664 (47) Zhang, B.; Zhang, L.; Li, F.; Hu, W.; Hannam, P.M. Testing the Formation of Ca–
665 Phosphonate Precipitates and Evaluating the Anionic Polymers as Ca–Phosphonate

Precipitates and $CaCO_3$ Scale Inhibitor in Simulated Cooling Water. *Corros. Sci.* **2010,** *52,* 3883-3890.

(48) Akyol, E.; Öner, M.; Barouda, E.; Demadis, K. D. Systematic Structural Determinants of the Effects of Tetraphosphonates on Gypsum Crystallization. *Cryst. Growth Des.* **2009,** *9*, 5145-5154.

(49) Shi, W.; Xia, M.; Lei, W.; Wang, F. Molecular Dynamics Study of Polyether Polyamino Methylene Phosphonates as an Inhibitor of Anhydrite Crystal. *Desalination* **2013,** *322*, 137-143.

(50) Leung, W. H.; Nancollas, G. H. Nitrilotri (Methylenephosphonic Acid) Adsorption on Barium Sulfate Crystals and Its Influence on Crystal Growth. *J. Cryst. Growth* **1978,** *44*, 163-167.

(51) Liu, S.; Nancollas, G. A Kinetic and Morphological Study of the Seeded Growth of Calcium Sulfate Dihydrate in the Presence of Additives. *J. Colloid Interface Sci.* **1975,** *52*, 593-601.

(52) Kushnir, J. The Coprecipitation of Strontium, Magnesium, Sodium, Potassium and Chloride Ions With Gypsum. an Experimental Study. *Geochim. Cosmochim. Acta* **1980,** *44*, 1471-1482.

(53) Rabizadeh, T.; Peacock, C. L.; Benning, L. G. Effectiveness of Green Additives vs Poly(acrylic acid) in Inhibiting Calcium Sulfate Dihydrate Crystallization, *Ind. Eng. Chem. Res.* **2019,** *58*, 1561–1569

(54) Weijnen, M.; Van Rosmalen, G. Adsorption of Phosphonates on Gypsum Crystals. *J. Cryst. Growth* **1986,** *79*, 157-168.

(55) Weijnen, M.; Van der Leeden, M.; Rosmalen, G. Influence of the Molecular Structure of Phosphonate Inhibitors on Various Aspects of Barite and Gypsum Crystallization. In proceeding of the international meeting *Geochemistry of the Earth's surface and*

691 *process of Mineral formation, Granada, Spain, March 16-22,* 1986; Rodriguez-
692 Clemente, R., Tardy, Y., Eds., CEP: Madrid, 1986..
693 (56) Zhang, G.; Yu, T. Coordination Adsorption of Anions. In *Chemistry of Variable Charge*
694 *Soils. Oxford Univ. Press, New York*, Yu, T., Ed. Oxford University Press: 1997; pp
695 175-218.
696 (57) Lee, S. Y.; Welbourn, R.; Clarke, S. M.; Skoda, M. W.; Clifton, L.; Zarbakhsh, A.
697 Adsorption of Sodium Hexanoate on α-Alumina. *J. Colloid Interface Sci.* **2013,** *407*,
698 348-353.
699 (58) Weijnen, M.P.C.; Van Rosmalen G.M. Adsorption of Phosphonates on Gypsum
700 Crystals. *J. Cryst. Growth*. **1986,** *79*, 157-168.
701 (59) Daniels, Y.; Lyczko, N.; Nzihou, A.; Alexandratos, S. D. Modification of
702 Hydroxyapatite With Ion-Selective Complexants: 1-Hydroxyethane-1, 1-
703 Diphosphonic Acid, *Ind. Eng. Chem. Res.* **2015,** *54*, 585-596.
704 (60) Bishop, M.; Bott, S. G.; Barron, A. R. A New Mechanism for Cement Hydration
705 Inhibition: Solid-State Chemistry of Calcium Nitrilotris (Methylene) Triphosphonate,
706 *Chem. Mater.* **2003,** *15*, 3074-3088.
707 (61) Kan, A. T.; Fu, G.; Tomson, M. B. Adsorption and Precipitation of an
708 Aminoalkylphosphonate Onto Calcite. *J. Colloid Interface Sci.* **2005,** *281*, 275-284.
709 (62) Vavouraki, A.; Koutsoukos, P. The Inhibition of Crystal Growth of Mirabilite in
710 Aqueous Solutions in the Presence of Phosphonates. *J. Cryst. Growth* **2016,** *436*, 92-
711 98.
712 (63) Ruiz-Agudo, E.; Rodriguez-Navarro, C.; Sebastián-Pardo, E. Sodium Sulfate
713 Crystallization in the Presence of Phosphonates: Implications in Ornamental Stone
714 Conservation. *Cryst. Growth Des.* **2006,** *6*, 1575-1583.

(64) Qian, B.; Wang, J.; Zheng, M.; Hou, B. Synergistic Effect of Polyaspartic Acid and Iodide Ion on Corrosion Inhibition of Mild Steel in H_2SO_4, *Corros. Sci.* **2013,** *75*, 184-192.

(65) Popov, K.; Maxim O.; Elena A.; Elena K.; Yulia D.; and Hannu R. A New Insight Into the Mechanism of the Scale Inhibition: Dls Study of Gypsum Nucleation in Presence of Phosphonates Using Nanosilver Dispersion as an Internal Light Scattering Intensity Reference, *Colloid Surf. A: Physicochem. Eng. Asp,* **2019**, *560*, 122-129.

(66) Rubbo, M.; Massaro, F.; Aquilano, D.; Vanzetti, W. Morphology of Gypsum: A Case Study. *Cryst. Res. Technol.* **2011,** *46*, 779-783.

(67) Li, F.; Liu, J.; Yang, G.; Pan, Z.; Ni, X.; Xu, H.; Huang, Q. Effect of pH and Succinic Acid on the Morphology of α-Calcium Sulfate Hemihydrate Synthesized by a Salt Solution Method. *J. Cryst. Growth* **2013,** *374*, 31-36.

(68) Montagnino, D.; Costa, E.; Massaro, F.; Artioli, G.; Aquilano, D. Growth Morphology of Gypsum in the Presence of Copolymers. *Cryst. Res. Technol.* **2011,** *46*, 1010-1018.

(69) Barouda, E.; Demadis, K. D.; Freeman, S. R.; Jones, F.; Ogden, M. I. Barium Sulfate Crystallization in the Presence of Variable Chain Length Aminomethylenetetraphosphonates and Cations (Na^+ or Zn^{2+}). *Cryst. Growth Des.* **2007,** *7*, 321-327.

738

739

740

741

742

743

744 **Table of Contents Graphic**

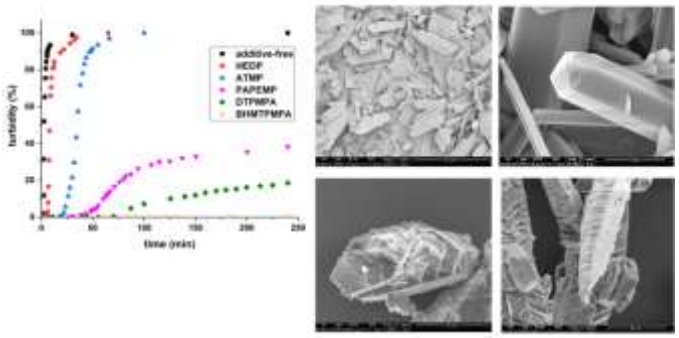

745

746

747

748

749